Superconducting transition temperature of the hole-doped cuprate as the stabilization temperature of supercurrent loops generated by spin-twisting itinerant motion of electrons

Akira Okazaki, Hikaru Wakaura, Hiroyasu Koizumi

*Division of Materials Science, University of Tsukuba,Tsukuba, Ibaraki 305-8573, Japan**

Michel Abou Ghantous

Department of Physics, Texas A & M University at Qatar,

Education City, PO Box 23875, Doha, Qatar†

Masashi Tachiki

Department of Physics, Tohoku University, Sendai, Miyagi 980-8578, Japan‡

(Dated: March 20, 2015)

Abstract

A theoretical calculation for the superconducting transition temperature of the hole doped cuprate is performed based on supercurrent generation by the spin-twisting itinerant motion of electrons. The superconducting transition temperature, T_c, is determined by a numerical simulation as the stabilization temperature of the coherence-length-sized loop currents, "spin-vortex-induced loop currents (SVILCs)", generated by the spin-twisting itinerant motion of electrons.

The simulation indicates that the stabilization of the SVILCs occurs in two steps; when temperature is decreased from room temperature, first, the phase where the sum of the winding numbers of the SVILCs is zero appears; with further decrease of the temperature, the phase where the winding numbers of the SVILCs are fixed appears. We identify the latter to the superconducting phase, and the former to the temperature below which the Kerr rotation is observed.

The calculated T_c value is close to the experimental value around the optimal doping. It scales as $\frac{t^2}{U}$ in a similar manner to the antiferromagnetic spin-fluctuation, where t is the nearest neighbor transfer integral and U is the on-site Coulomb repulsion parameter. The calculated T_c disagrees in the underdoped and overdoped regions. These disagreements are explained as due to the reduction of T_c by the quantum criticality arising from the two quantum critical points at the lowest and highest ends of the hole density x of the superconducting phase, where the former corresponds to the percolation threshold of the spin-vortices, and the latter to the spin-vortex formation-destruction critical point.

PACS numbers: 74.72.-h,74.72.Gh

*koizumi@ims.tsukuba.ac.jp

†michel.aboughantous@qatar.tamu.edu

‡tachiki@cmpt.phys.tohoku.ac.jp

I. INTRODUCTION

Accumulating experimental results indicate that the BCS theory is not capable of explaining the superconductivity in the cuprates. For example, a theoretical estimate revealed that the superconducting transition temperature T_c is not determined by the energy gap formation as in the BCS superconductor [1], but corresponds to the stabilization temperature of the coherence-length-sized persistent loop currents [2]. The STM experiment has observed that the superconducting transition temperature is determined by the percolation of nano-sized superconducting regions [3].

Since the single-particle dispersion of the energy band structure is observed by the ARPES experiment, it is tempting to consider that the Cooper pair formation of the band electrons is the origin of the superconductivity [4]. However, since the ARPES results reflect largely the electronic state in the surface region, the bulk electronic state may be different from the one derived throughly by the ARPES experiment. Indeed, other experimental methods indicate the intimate relation between the superconductivity and the inhomogeneity of the bulk electronic state, which is difficult to be observed by the ARPES experiment. The inhomogeneity in the electronic state is vividly observed in the STM experiment [5]; the inelastic neutron scattering experiment reveals the existence of the charge and spin inhomogeneity [6]; and the EXAFS indicates the relation between the superconductivity and inhomogeneous Cu-O bond length fluctuations [7, 8]. Further, the enhanced Nernst signals and the magnetic Kerr effect measurement indicate that the existence of loop currents in the pseudogap phase above the superconducting transition temperature T_c [9, 10].

A new theory of superconductivity based on spin-twisting itinerant motion of electrons was put forward by the present authors [11–16]. This theory explains the relation between the superconductivity and inhomogeneous electronic states, including the appearance of the Cu-O bond length fluctuations and stable loop currents. In this theory, the appearance of the superconducting state is explained due to the network formation and stabilization of the coherence-length-sized persistent loop currents produced by the spin-twisting itinerant motion of electrons. The loop current generated by the spin-twisting itinerant motion of electrons is called the 'spin-vortex-induced loop-current (SVILC)', and the stabilization of the spin-vortices is required. The doped holes become the stabilizing centers of the spin-vortices by providing their cores and the superexchange interaction between electrons across

hole occupied sites.

Although the occurrence of the superconductivity in the new mechanism is not related to the Cooper pair formation, it explains the flux quantum $hc/2e$ and the Josephson frequency $2eV/h$ [11, 14, 15]. It is also noteworthy that this theory is applicable to the BCS superconductors if the Rashba spin-orbit interaction is added to the BCS Hamiltonian; in this case, the Cooper pair is composed of time-reversal partners of the spin-twisting itinerant electrons [15, 16]. This extension suggests that the appearance of the spin-twisting itinerant motion of electrons is more fundamental to the supercurrent generation than the Cooper pair formation.

In the new theory [11–16], the ultimate origin of the supercurrent generation is attributed to the single-valued requirement of the wave function, which gives rise to the forced whole system motion. It is effective even in the Mott insulator, and explains the current generation in the cuprates. The superconducting wave function in this theory is given in the following form

$$\Psi(\mathbf{r}^{(1)},\cdots,\mathbf{r}^{(N)}) = \Psi_0(\mathbf{r}^{(1)},\cdots,\mathbf{r}^{(N)})e^{-\frac{i}{2}\sum_{\alpha=1}^{N}\chi(\mathbf{r}^{(\alpha)})} \tag{1}$$

where $\mathbf{r}^{(\alpha)}$ is the coordinate of the αth electron and N is the total number of electrons. Ψ_0 is a currentless multi-valued wave function, where the multi-valuedness arises from the spin-twisting of the itinerant electrons. The phase factor $e^{-\frac{i}{2}\sum_{\alpha=1}^{N}\chi(\mathbf{r}^{(\alpha)})}$ is crucial to fulfill the single-valued requirement of the total wave function, where χ is an angular variable of period 2π [13–16]. The phase factor $e^{-\frac{i}{2}\sum_{\alpha=1}^{N}\chi(\mathbf{r}^{(\alpha)})}$ gives rise to the current which cannot be obtained by the perturbation theory.

Due to the phase factor $e^{-\frac{i}{2}\sum_{\alpha=1}^{N}\chi(\mathbf{r}^{(\alpha)})}$ in the wave function, the vector potential of electromagnetic field $\mathbf{A}^{\rm em}$ always appear in the following combination,

$$\mathbf{A}^{\rm eff} = \mathbf{A}^{\rm em} - \frac{c\hbar}{2e}\nabla\chi. \tag{2}$$

It is gauge invariant due to the fact that $\nabla\chi$ is optimized; i.e., if a different gauge is adopted for the vector potential, $\mathbf{A}^{\rm em} \to \mathbf{A}^{\rm em} + \nabla f$, the optimized $\nabla\chi$ becomes $\nabla\chi \to \nabla\chi + \frac{2e}{c\hbar}\nabla f$; thus, $\mathbf{A}^{\rm eff}$ is invariant by the change of the gauge.

The time-component partner of $\mathbf{A}^{\rm eff}$ is given by

$$\varphi^{\rm eff} = \varphi^{\rm em} + \frac{\hbar}{2e}\frac{\partial\chi}{\partial t}; \tag{3}$$

it is also gauge invariant, where $\varphi^{\rm em}$ is the scalar potential of electromagnetic field. The above two effective gauge potentials explain the flux quantum $hc/2e$ and the Josephson frequency $2eV/h$ without Cooper pairs [11, 13–15]. It is also noteworthy that the re-derivation of the Josephson effects using the new theory suggest that the currently-accepted supercurrent generation mechanism that attributes the supercurrent to the flow of the Cooper pairs that couple to the vector potential pairwise may be incorrect [15].

For the BCS superconductors, T_c is determined as the energy gap formation temperature by the Cooper pair formation. In the present work, we show that it is given as the stabilization temperature of the SVILCs in the cuprates. The calculated transition temperature T_c is shown to give a reasonable value around the optimal doping.

The organization of the present work is as follows: in the next section, the mechanism of the supercurrent generation by the spin-twisting itinerant motion of electrons is briefly summarized, and the order parameter for the superconducting state is given. In Section III, the way to obtain the energy functional $E[\nabla\chi]$ is explained; this functional is utilized to obtain χ in the wave function. In Section IV, the Monte Carlo simulation for the SVILC stabilization is described; the result yields a reasonable T_c value around the optimal doping, however, it disagrees in the underdoped and overdoped regions. In Section V, we argue that the disagreement of T_c values in the underdoped and overdosed regions are due to the reduction of T_c by the quantum criticality arising from the quantum critical points at the lowest and highest ends of the hole density x for the superconducting phase. In Section VI, we conclude the present work.

II. SUPERCURRENT GENERATION BY THE SPIN-TWISTING ITINERANT MOTION OF ELECTRONS, AND SUPERCONDUCTING STATE ORDER PARAMETER

In the new theory, the superconducting wave function is given in Eq. (1); the angular variable χ in it is determined by the optimization of the following functional

$$F[\nabla\chi] = E[\nabla\chi] + \sum_{\ell=1}^{N_{\rm loop}} \lambda_\ell \left(\oint_{C_\ell} \nabla\chi \cdot d\mathbf{r} - 2\pi\bar{w}_\ell \right) \tag{4}$$

where $E[\nabla\chi]$ is the energy functional of $\nabla\chi$ given by

$$E[\nabla\chi] = \langle\Psi|H[\mathbf{A}^{\rm em}]|\Psi\rangle = \langle\Psi_0|H[\mathbf{A}^{\rm em} - \frac{c\hbar}{2e}\nabla\chi]|\Psi_0\rangle = E^{\rm super}[\mathbf{A}^{\rm em} - \frac{c\hbar}{2e}\nabla\chi]; \tag{5}$$

$H[\mathbf{A}^{\rm em}]$ is the Hamiltonian with the electromagnetic vector potential $\mathbf{A}^{\rm em}$; λ_ℓ is the Lagrange multiplier to impose the constraint

$$\oint_{C_\ell} \nabla\chi \cdot d\mathbf{r} = 2\pi\bar{w}_\ell, \tag{6}$$

$N_{\rm loop}$ is the minimal number of loops with which any loops in the system can be constructed, and $\bar{w}_\ell$ is integer specified by the boundary condition and the single-valued requirement of the wave function [13, 14]. The meaning of the above constraint is explained in the next section.

The current density is generally expressed using the energy functional $E[\nabla\chi] = E^{\rm super}[\mathbf{A}^{\rm em} - \frac{c\hbar}{2e}\nabla\chi]$ as

$$\mathbf{j} = -c\frac{\delta E^{\rm super}[\mathbf{A}^{\rm em} - \frac{c\hbar}{2e}\nabla\chi]}{\delta \mathbf{A}^{\rm em}} = \frac{2e}{\hbar}\frac{\delta E^{\rm super}[\mathbf{A}^{\rm em} - \frac{c\hbar}{2e}\nabla\chi]}{\delta\nabla\chi} = \frac{2e}{\hbar}\frac{\delta E[\nabla\chi]}{\delta\nabla\chi}. \tag{7}$$

The stationary condition of $F[\nabla\chi]$, $\frac{\delta F[\nabla\chi]}{\delta\nabla\chi} = 0$, yields the following relation,

$$\frac{\delta E[\nabla\chi]}{\delta\nabla\chi} = -\sum_{\ell=1}^{N_{\rm loop}} \lambda_\ell \frac{\delta}{\delta\nabla\chi}\oint_{C_\ell} \nabla\chi \cdot d\mathbf{r}. \tag{8}$$

Thus, the current density is expressed as

$$\mathbf{j} = -\frac{2e}{\hbar}\sum_{\ell=1}^{N_{\rm loop}} \lambda_\ell \frac{\delta}{\delta\nabla\chi}\oint_{C_\ell} \nabla\chi \cdot d\mathbf{r}. \tag{9}$$

This is the supercurrent density in the new theory. It is a sum of loop currents called, the 'spin-vortex-induced loop-currents (SVILCs)'. The current density is obtained either by evaluating λ_ℓ's or calculating the expectation value of the current density operator with the wave function in Eq. (1) [14].

The current in Eq. (9) is nonzero if some of $\bar{w}_\ell$ ($\ell = 1, \cdots, N_{\rm loop}$) are not zero, and the following condition is satisfied,

$$\frac{\delta E[\nabla\chi]}{\delta\nabla\chi} \neq 0. \tag{10}$$

This current can flow even in the band insulator or Mott insulator if the above mentioned conditions are satisfied unlike the conventional one obtained by the linear response theory.

The order parameter of the superconducting state is identified if we consider the supercurrent generation with the current feeding boundary condition. The current feeding boundary

condition is realized by adding external loops, where the external loops the loops that contain paths connecting the flow-in and flow-out sites of the feeding currents. Including the external loops, the functional to be optimized is given by

$$\begin{aligned} F^{\rm ext}[\nabla\chi] &= E[\nabla\chi] + \sum_{\ell=1}^{N_{\rm loop}} \lambda_\ell \left(\oint_{C_\ell} \nabla\chi \cdot d\mathbf{r} - 2\pi\bar{w}_\ell \right) \\ &+ \sum_{\ell=1}^{N_{\rm loop}^{\rm ext}} \lambda_\ell^{\rm ext} \oint_{C_\ell^{\rm ext}} \nabla\chi \cdot d\mathbf{r} \end{aligned} \tag{11}$$

where $\lambda_\ell^{\rm ext}$ is an externally supplied parameter that depends on the feeding currents, and $C_\ell^{\rm ext}$ is an external loop; actually, $\lambda_\ell^{\rm ext}$ is related to the feeding current $\mathbf{j}^{\rm ext}$ as

$$\mathbf{j}^{\rm ext} = -\frac{2e}{\hbar} \sum_{\ell=1}^{N_{\rm loop}^{\rm ext}} \lambda_\ell^{\rm ext} \frac{\delta}{\delta\nabla\chi} \oint_{C_\ell^{\rm ext}} \nabla\chi \cdot d\mathbf{r}, \tag{12}$$

in analogous to Eq. (9).

For a given state with the wave function of the from in Eq. (1), the constraint in Eq. (11) is satisfied, thus, the energy becomes

$$\begin{aligned} E^{\rm ext}[\nabla\chi] &= E[\nabla\chi] + \sum_{\ell=1}^{N_{\rm loop}^{\rm ext}} \lambda_\ell^{\rm ext} \oint_{C_\ell^{\rm ext}} \nabla\chi \cdot d\mathbf{r} \\ &= E[\nabla\chi] + \sum_{\ell=1}^{N_{\rm loop}^{\rm ext}} \lambda_\ell^{\rm ext} \oint_{S_\ell^{\rm ext}} \nabla\times\nabla\chi \cdot d\mathbf{S}, \end{aligned} \tag{13}$$

where $S_\ell^{\rm ext}$ is the surface with $C_\ell^{\rm ext}$ as perimeter. From Eq. (13), we may identify $\nabla\times\nabla\chi$ as the order parameter, and $\{\lambda_\ell^{\rm ext}\}$ as its conjugate field. The points of $\nabla\times\nabla\chi \neq 0$ are singularities of χ. They are detected by calculating the winding number of χ around loop C_ℓ, $w_\ell[\chi](\ell = 1, \cdots, N_{\rm loop})$, defined as

$$w_\ell[\chi] = \frac{1}{2\pi} \oint_{C_\ell} \nabla\chi \cdot d\mathbf{r}. \tag{14}$$

We identify in the following that the superconducting phase is the one with

$$\langle w_\ell[\chi] \rangle_{\rm T} \neq 0 \tag{15}$$

without feeding current ($\lambda_\ell^{\rm ext} = 0$) or external magnetic field ($\mathbf{A}^{\rm em} = 0$), where $\langle \hat{O} \rangle_{\rm T}$ indicates the thermal average of $\hat{O}$.

III. CALCULATION OF $E[\nabla\chi]$

In order to obtain the wave function of the superconducting state, the energy functional $E[\nabla\chi]$ is needed. For that purpose, we use a model Hamiltonian for electrons in the CuO_2 plane of the cuprate.

The model Hamiltonian for the hole doped cuprates may be given by

$$H_{\rm EHFS} = -\sum_{\langle i,j\rangle_1,\sigma} t(c^\dagger_{i\sigma}c_{j\sigma}+c^\dagger_{j\sigma}c_{i\sigma})+U\sum_j c^\dagger_{j\uparrow}c_{j\uparrow}c^\dagger_{j\downarrow}c_{j\downarrow} + J'\sum_{\langle i,j\rangle_h}\hat{\mathbf{S}}_i\cdot\hat{\mathbf{S}}_j + H_{h-h} \qquad (16)$$

where i and j are sites in the two-dimensional square lattice in the CuO_2 plane where copper atoms reside. We assume that in the bulk of the cuprate, doped holes become small lattice polarons, and their mobility becomes very small. We take the extreme limit where the doped holes become immobile small polarons, and exclude sites occupied by the holes in the sums in Eq. (16). The sum of $\langle i,j\rangle_1$ in the first term indicates that the sum is taken over the nearest neighbor pairs. The sum of $\langle i,j\rangle_h$ in the third term indicates that the sum is taken over the pairs across the hole occupied sites. Oxygens that exist between nearest neighbor coppers are not explicitly taken into account. $c^\dagger_{j\sigma}$ and $c_{j\sigma}$ are the creation and annihilation operators of electrons at the jth site with the z-axis projection of electron spin σ, respectively; $\hat{\mathbf{S}}_j$ is the spin moment operator at the jth site given by

$$\hat{\mathbf{S}}_j = \frac{1}{2}\sum_{\sigma,\sigma'} c^\dagger_{j\sigma}\boldsymbol{\sigma}_{\sigma\sigma'}c_{j\sigma'} \qquad (17)$$

$\boldsymbol{\sigma}$ is the vector of Pauli matrices. The last term H_{h-h} describes the Coulomb repulsion between holes which prohibits the appearance of next neighbor hole pairs.

Although the term with J' in Eq (16) is important in the stabilization of the spin-vortices we omit it in the following since we construct an ensemble by keeping the spin-configuration and only by changing the winding number for χ. The effect of the last term in Eq (16) is taken into account by placing the holes so that the nearest neighbor holes do not appear. The rest of the Hamiltonian is replaced by the following self-consistent Hamiltonian given by

$$\begin{aligned} H^{HF}_{\rm EHFS} &= -t\sum_{\langle i,j\rangle_1,\sigma}\left(c^\dagger_{i\sigma}c_{j\sigma}+c^\dagger_{j\sigma}c_{i\sigma}\right) \\ &+ U\sum_j\Big[(\frac{n_j}{2}-S^z_j)c^\dagger_{j\uparrow}c_{j\uparrow}+(\frac{n_j}{2}+S^z_j)c^\dagger_{j\downarrow}c_{j\downarrow}-(S^x_j-iS^y_j)c^\dagger_{j\uparrow}c_{j\downarrow}-(S^x_j+iS^y_j)c^\dagger_{j\downarrow}c_{j\uparrow}\Big] \end{aligned} \qquad (18)$$

where n_j is the electron number at the jth site,

$$n_j = \sum_\sigma \langle c^\dagger_{j\sigma} c_{j\sigma} \rangle, \tag{19}$$

S^x_j, S^y_j, andS^z_j are components of electron spin at the jth site given by

$$\begin{aligned} S^x_j &= \frac{1}{2}\langle c^\dagger_{j\uparrow} c_{j\downarrow} + c^\dagger_{j\downarrow} c_{j\uparrow} \rangle = S_j \cos\xi_j \sin\zeta_j \\ S^y_j &= -\frac{i}{2}\langle c^\dagger_{j\uparrow} c_{j\downarrow} - c^\dagger_{j\downarrow} c_{j\uparrow} \rangle = S_j \sin\xi_j \sin\zeta_j \\ S^z_j &= \frac{1}{2}\langle c^\dagger_{j\uparrow} c_{j\uparrow} - c^\dagger_{j\downarrow} c_{j\downarrow} \rangle = S_j \cos\zeta_j \end{aligned} \tag{20}$$

where ξ and ζ are expressed by the azimuth and polar angle angles, respectively; $\langle \hat{O} \rangle$ denotes the expectation value of the operator $\hat{O}$. Since the numerical calculations revealed the stability of $\zeta = \pi/2$ for all sites, we use this value in the present work. By this choice, the spins are lying in the CuO_2 plane [13, 14].

The self-consistent results obtained must be supplemented by the single-valued requirement of the wave function. In the following, we describe the way we impose the single-valued requirement of the wave function. Let us introduce an angular variable η to describe the spin-vortices in the antiferromagnetic background. The background antiferromagnetic spin is given by $\xi_j = \pi(j_x + j_y)$, where (j_x, j_y) is the x-y coordinates of the jth site taking the lattice constant $a = 1$. We define η_j as

$$\eta_j = \xi_j - \pi(j_x + j_y) \tag{21}$$

and separate the background antiferromagnetic contribution. The difference of η between nearest neighbor sites is taken in the range,

$$-\pi \leq \eta_\ell - \eta_k < \pi. \tag{22}$$

The winding number of η for loop C_ℓ is defined as

$$w_\ell[\eta] = \frac{1}{2\pi} \sum_{i=1}^{N_\ell} (\eta_{C_\ell(i+1)} - \eta_{C_\ell(i)}) \tag{23}$$

where C_ℓ is a loop in the x-y plane. N_ℓ is the total number of sites on the loop C_ℓ, and $C_\ell(i)$ is the ith site on it with the periodic condition $C_\ell(N_\ell + 1) = C_\ell(1)$. The presence of spin-vortices is characterized by the non-zero value for some of $w_\ell[\eta]$'s.

From the above self-consistent calculation, we obtain the phase differences of ξ, such as $\xi_i - \xi_j$. From these phase differences, we can construct ξ and calculate the winding number

$$w_\ell[\xi] = \frac{1}{2\pi}\sum_{i=1}^{N_\ell}(\xi_{C_\ell(i+1)} - \xi_{C_\ell(i)}) \tag{24}$$

If the loop C_ℓ encircles a spin-vortex with the winding number $w_\ell[\xi]$, ξ has a jump of value by $2\pi w_\ell[\xi]$. This jump of value may cause the multi-valuedness problem of wave functions.

To see the multi-valuedness problem of the wave function arising from the spin vortices, we introduce the new creation operators $a_j^\dagger$ and $b_j^\dagger$ that have spin-quantization axis in the direction of $\mathbf{S}_j = (S_j^x, S_j^y, S_j^z)$; they are related to $c_{j\sigma}^\dagger$ by

$$\begin{aligned} a_j^\dagger &= e^{-i\frac{\chi_j}{2}}\left(\cos\frac{\zeta_j}{2}e^{-i\frac{\xi_j}{2}}c_{j\uparrow}^\dagger + \sin\frac{\zeta_j}{2}e^{i\frac{\xi_j}{2}}c_{j\downarrow}^\dagger\right) = \frac{e^{-i\frac{\chi_j}{2}}}{\sqrt{2}}\left(e^{-i\frac{\xi_j}{2}}c_{j\uparrow}^\dagger + e^{i\frac{\xi_j}{2}}c_{j\downarrow}^\dagger\right) \\ b_j^\dagger &= e^{-i\frac{\chi_j}{2}}\left(-\sin\frac{\zeta_j}{2}e^{-i\frac{\xi_j}{2}}c_{j\uparrow}^\dagger + \cos\frac{\zeta_j}{2}e^{i\frac{\xi_j}{2}}c_{j\downarrow}^\dagger\right) = \frac{e^{-i\frac{\chi_j}{2}}}{\sqrt{2}}\left(-e^{-i\frac{\xi_j}{2}}c_{j\uparrow}^\dagger + e^{i\frac{\xi_j}{2}}c_{j\downarrow}^\dagger\right). \end{aligned} \tag{25}$$

The phase factor $e^{-i\frac{\chi_j}{2}}$ is added to impose the single-valued requirement of the wave function; since the phase factors $e^{\pm i\frac{\xi_j}{2}}$ becomes $e^{\pm i\frac{\xi_j}{2}\pm i\pi w_\ell[\xi]}$ after the excursion along loop C_ℓ, the sign change of the wave function occurs if $w_\ell[\xi]$ is odd. By imposing the following constraint

$$w_\ell[\xi] + w_\ell[\chi] = \text{even number for any loop } C_\ell \tag{26}$$

the phase factor $e^{-\frac{i}{2}\chi}$ compensates this sign change, making the basis in Eq. (25) single-valued.

In oder to obtain χ that satisfies the above condition, we do the following: first, we introduce the following new basis to separate the multi-valued phase factors $e^{\pm i\frac{\xi_j}{2}}$;

$$\begin{aligned} \tilde{d}_{j\uparrow} &= e^{i\frac{\xi_j}{2}}c_{j\uparrow}, \\ \tilde{d}_{j\downarrow} &= e^{-i\frac{\xi_j}{2}}c_{j\downarrow} \end{aligned} \tag{27}$$

Then, the Hartree-Fock Hamiltonian becomes

$$\begin{aligned} H_{\text{EHFS}}^{HF} &= -t\sum_{\langle i,j\rangle_1}\left(e^{\frac{i}{2}(\xi_i-\xi_j)}\tilde{d}_{i\uparrow}^\dagger\tilde{d}_{j\uparrow} + e^{-\frac{i}{2}(\xi_i-\xi_j)}\tilde{d}_{i\downarrow}^\dagger\tilde{d}_{j\downarrow} + \text{h.c.}\right) \\ &+ U\sum_j\Big[(\frac{n_j}{2} - S_j^z)\tilde{d}_{j\uparrow}^\dagger\tilde{d}_{j\uparrow} + (\frac{n_j}{2} + S_j^z)\tilde{d}_{j\downarrow}^\dagger\tilde{d}_{j\downarrow} - (S_j^x - iS_j^y)e^{i\xi_j}\tilde{d}_{j\uparrow}^\dagger\tilde{d}_{j\downarrow} \\ &- (S_j^x + iS_j^y)e^{-i\xi_j}\tilde{d}_{j\downarrow}^\dagger\tilde{d}_{j\uparrow}\Big] \end{aligned} \tag{28}$$

By self-consistently diagonalizing the above Hamiltonian, we again obtain the multi-valued basis function;

$$\begin{aligned} |\tilde{\gamma}\rangle &= \sum_j [D^{\gamma}_{j\uparrow}\tilde{d}^{\dagger}_{j\uparrow} + D^{\gamma}_{j\downarrow}\tilde{d}^{\dagger}_{j\downarrow}]|\mathrm{vac}\rangle \\ &= \sum_j [e^{-i\frac{\xi_j}{2}} D^{\gamma}_{j\uparrow} c^{\dagger}_{j\uparrow} + e^{i\frac{\xi_j}{2}} D^{\gamma}_{j\downarrow} c^{\dagger}_{j\downarrow}]|\mathrm{vac}\rangle \end{aligned} \tag{29}$$

The phase factors $e^{\pm i\frac{\xi_j}{2}}$ are separated, and single-valued coefficients $D^{\gamma}_{j\sigma}$'s are obtained.

By adding the phase factor introducing $e^{-i\frac{\chi}{2}}$, the single-valued wave functions are constructed as follows,

$$|\gamma\rangle = \sum_j e^{-i\frac{\chi_j}{2}} [e^{-i\frac{\xi_j}{2}} D^{\gamma}_{j\uparrow} c^{\dagger}_{j\uparrow} + e^{i\frac{\xi_j}{2}} D^{\gamma}_{j\downarrow} c^{\dagger}_{j\downarrow}]|\mathrm{vac}\rangle \tag{30}$$

The energy functional $E[\nabla\chi]$ is obtained as the total energy using the single Slater determinant composed of $|\gamma\rangle$.

IV. MONTE CARLO SIMULATIONS OF SPIN-VORTEX-INDUCED LOOP CURRENTS

In the new mechanism, there are three requirements for the appearance of superconducting state;

1. Generation of spin-vortices with doped holes as their cores (spin-vortex formation problem)
2. Creation of a network of spin-vortices (percolation problem)
3. Stabilization of the loop currents created around spin-vortices (loop-current stabilization problem)

In the following, we assume that the first and second requirements are already satisfied, and estimate T_c as a temperature where the third requirement (loop-current stabilization problem) is fulfilled. We perform Mote Carlo simulations using the Metropolis algorithm to deal with the fluctuation of the winding numbers of the SVILCs.

Before starting the Monte Carlo simulation, the following preparations are performed:

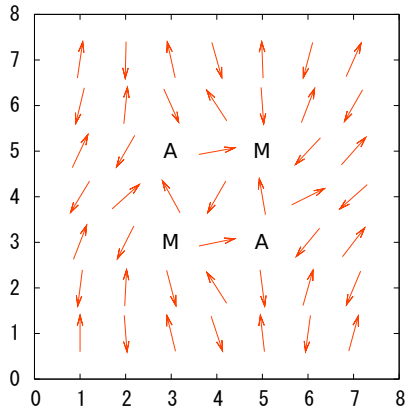

FIG. 1: The spin-vortex-quartet (SVQ). "M" and "A" denote the centers of the spin vortex with the winding number $+1$ and -1, respectively.

1. Arrange initial spin-vortices by specifying the centers of them and initial ξ_j values.

2. Solve the self-consistent field equations. Obtain the parameters for single-particle wave functions, $D^{\gamma}_{j\sigma}$'s and ξ_j's.

As a stable unit of spin-vortices, we used the spin-vortex-quartet (SVQ) shown in Fig. 1. It is stable since the deviation from the antiferromagnetic order is confined in a small region. The absence of the next neighbor hole pairs in the SVQ satisfies the requirement from H_{h-h} in Eq. (16).

In Fig. 2, four spin-vortex patterns we will employ for the simulation are depicted. The spin-vortex-quartets, $4a \times 4a$ units of four spin-vortices (two with "M" and two with "A") are tiled in cross-stripe fashion, where a is the lattice constant.

Next, the Metropolis algorithm is performed in the following steps to deal with the fluctuation of the current patterns:

1. The ground state is obtained by setting the winding numbers of χ equal to those of ξ ($\bar{w}_\ell$=$w_\ell[\xi]$ in Eq. (4)), and performing the constrained minimization of the energy using the functional $F[\nabla\chi]$ to obtain χ (see Fig. 3).

2. A trial state is constructed by the following two ways:

   - pick one $\bar{w}_\ell$, change sign ($\bar{w}_\ell \to -\bar{w}_\ell$), and obtain the optimized χ for $F[\nabla\chi]$ in Eq. (4). Using the new χ, the total electronic energy is calculated with the Slater

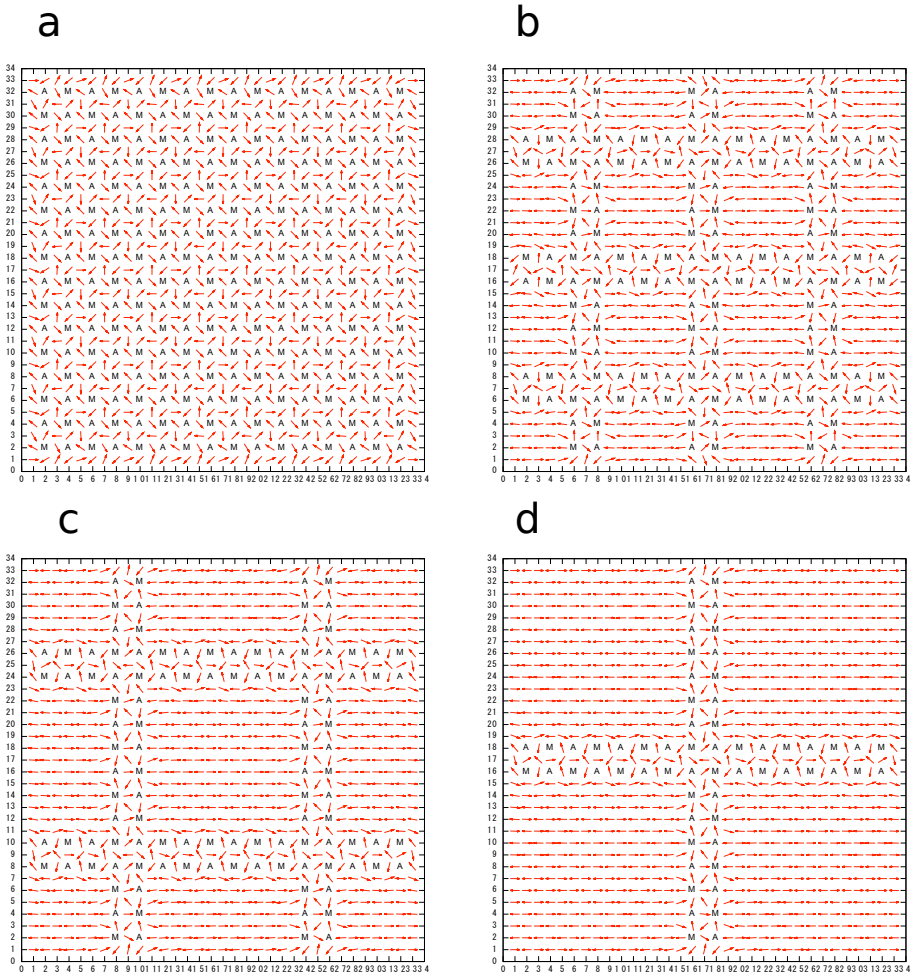

FIG. 2: Four spin-vortex patterns employed for the Monte Carlos simulation. "M" and "A" denote the centers of the spin vortex with the winding number $+1$ and -1, respectively. The spin-vortex-quartets (SVQs) are tiled in crossed-stripe forms in the 33×33 square lattice. **a**) 64 SVQ system ($x = 0.25$); **b**) 39 SVQ system ($x = 0.152$); **c**) 30 SVQ system ($x = 0.117$); **d**) 15 SVQ system ($x = 0.0586$), where x is given by $x = 4 \times$ (The number of SVQs)$/(32 \times 32)$.

determinant composed of the new single particle wave functions in Eq. (30) and the Hamiltonian in Eq. (18).

- pick two $\bar{w}_\ell$ and $\bar{w}_k$, exchange them ($\bar{w}_\ell \to \bar{w}_k$, $\bar{w}_k \to \bar{w}_\ell$), and obtain the optimized χ $F[\nabla\chi]$ in Eq. (4). Using the new χ, the total electronic energy is calculated with the Slater determinant composed of the new single particle wave functions in Eq. (30) and the Hamiltonian in Eq. (18).

3. Set the new state according to the Metropolis algorithm by comparing the energy of

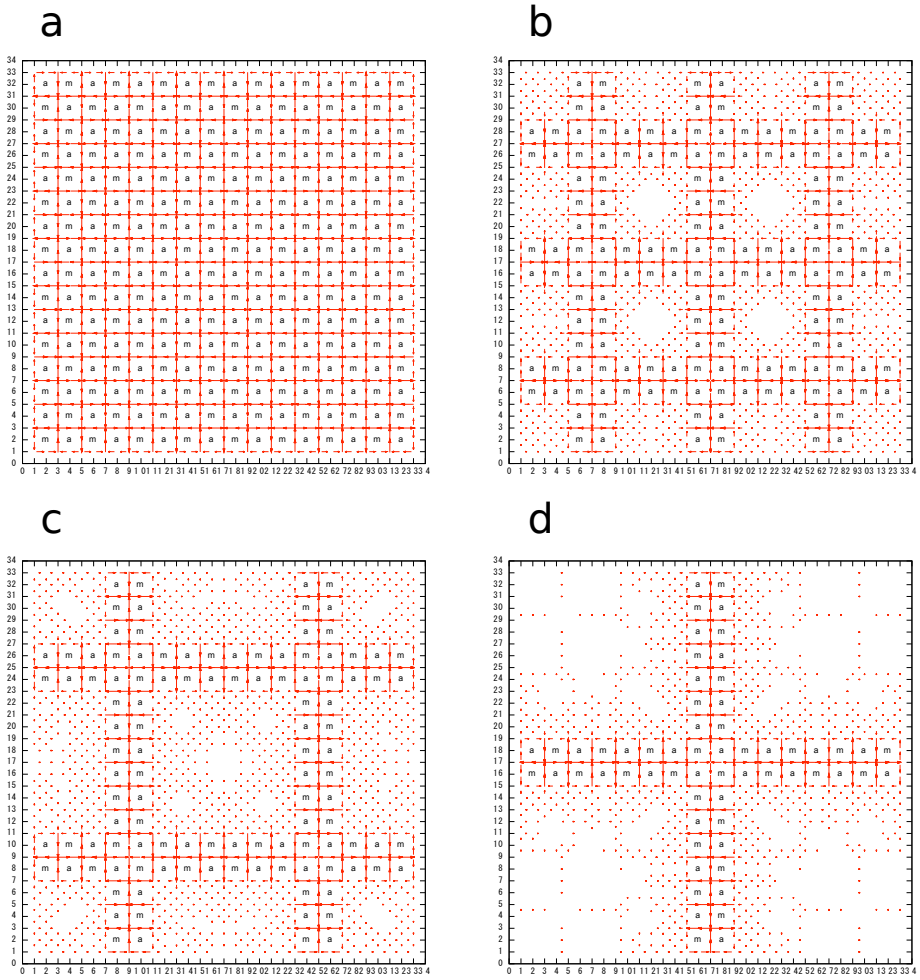

FIG. 3: Current patterns for the ground states. "m" and "a" denote the centers of the SVILCs with the winding number $+1$ and -1, respectively. Their spin configurations are depicted in Fig. 2.

the previous state and that of the trial state.

Using the ensembles generated by the above method, we calculate the heat capacity

$$C = \frac{1}{k_B T^2} \left(\langle E^2 \rangle_T - \langle E \rangle_T^2 \right), \tag{31}$$

where E is the total energy.

In order to detect the stability of the loop currents, we calculate the ensemble average of the deviation of the winding numbers of χ from the ground state values,

$$W_{\rm dev} = \langle \sum_{j=1}^{N_{\rm hole}} (w_j[\xi] - w_j[\chi])^2 \rangle_T, \tag{32}$$

where $N_{\rm hole}$ is the number of holes, $w_j[\xi]$ and $w_j[\chi]$ are the winding numbers of ξ and χ around the jth hole (only the jth hole exists within the loop for the winding number

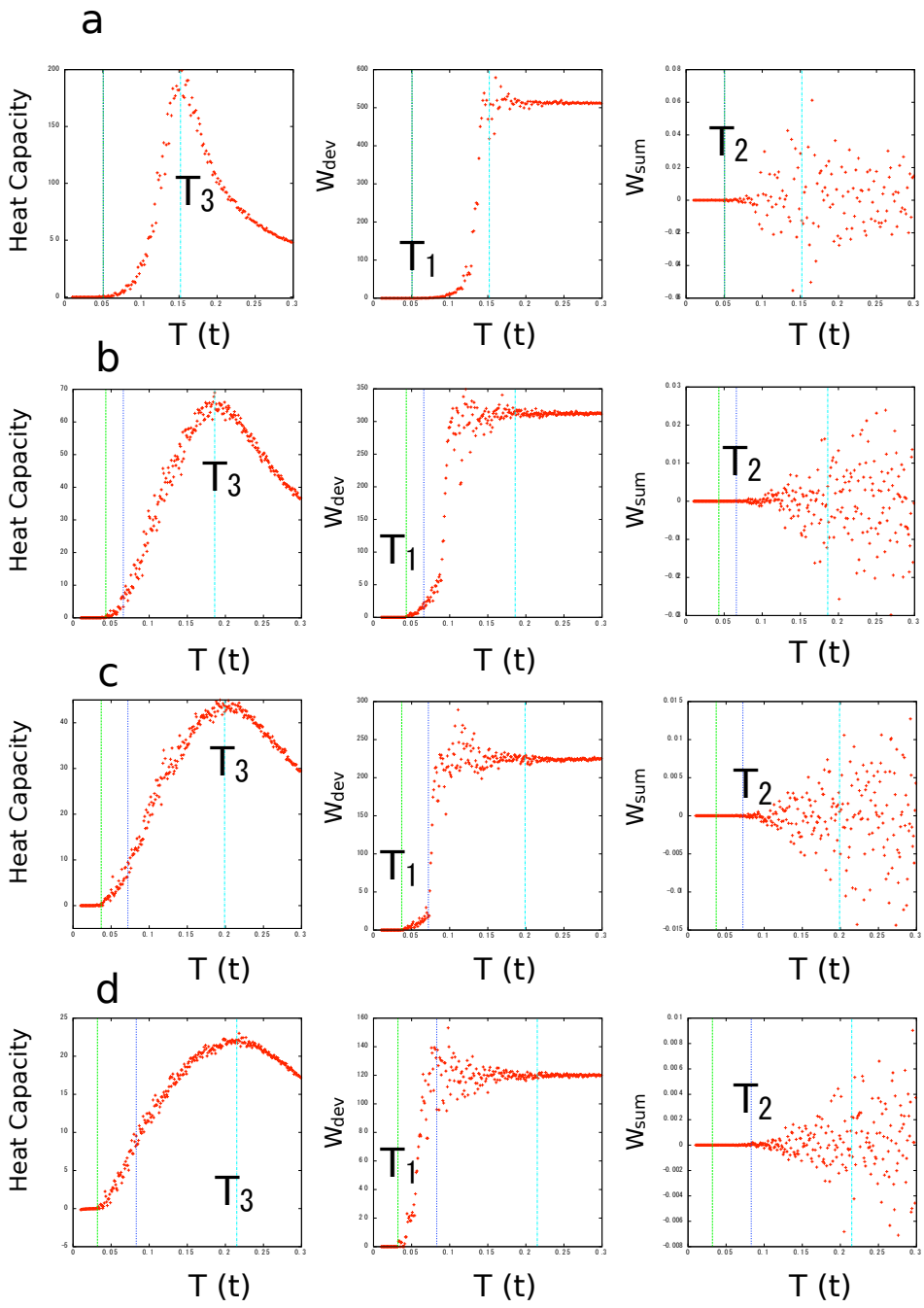

FIG. 4: Temperature, T, dependences of the heat capacity C (left), the average of the sum of the deviations of the winding numbers of χ from the ground state values, $W_{\rm dev}$ (middle), and the average of the sum of the winding numbers of χ, $W_{\rm sum}$ (right). The units of the temperature and energy are t. $U = 8t$. **a**) $x = 0.25$; **b**) $x = 0.152$; **c**) $x = 0.117$; **d**) $x = 0.0586$. T_1 is the temperature where $W_{\rm dev}$ starts non-zero, T_2 as the temperature where $W_{\rm sum}$ starts non-zero, and T_3 as the peak position of the heat capacity. The spin configurations are shown in Fig. 2.

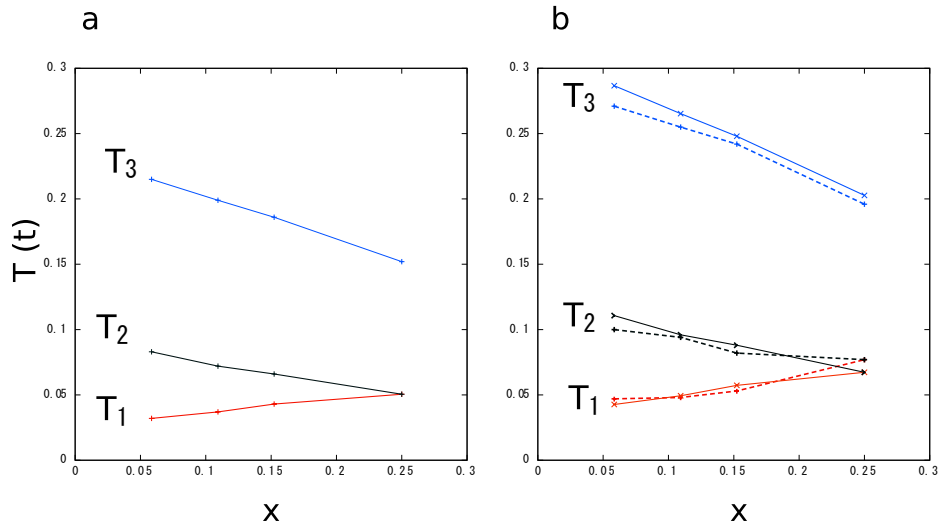

FIG. 5: The hole concentration x dependence of T_1, T_2, and T_3. **a**) $U = 8t$ results. **b**) $U = 6t$ results (dotted lines) and $U = 8t$ results multiplied by $\frac{8}{6}$ (sold lines).

calculation), respectively. Since for the ground state, we chose the one with $w_j[\chi] = w_j[\xi]$, thus, $W_{\rm dev}$ is the measure of the deviation from the ground state values. Note that the ensembles at different temperatures are obtained successively by raising the temperature.

We also calculate the ensemble average of the sum of the winding numbers of χ given by

$$W_{\rm sum} = \langle \sum_{j=1}^{N_{\rm hole}} w_j[\chi] \rangle_T. \tag{33}$$

The results are displayed in Fig. 4. Three temperatures are defined: T_1 is defined as the temperature where $W_{\rm dev}$ starts nonzero, T_2 as the temperature where $W_{\rm sum}$ starts nonzero, and T_3 as the peak position of the heat capacity. They satisfy $T_1 \leq T_2 < T_3$. Fig. 4 shows that T_1 also corresponds to the temperature where the heat capacity starts to rise. Below T_1 the current pattern is fixed. We identify T_1 as the superconducting transition temperature T_c. Below T_2 the sum of the winding numbers the loop currents is zero; at this temperature, the winding numbers of the loop currents do not change except by the exchange of the winding numbers of two loop currents. We regard T_2 corresponds to the temperature $T_{\rm K}$ bellow which the Kerr rotation is observed [10]. Above T_3, the winding numbers of the loop currents are random, indicating that loop currents are no more detectable.

The hole concentration dependence of T_1, T_2, and T_3 are depicted in Fig. 5. In real material, T_c is zero below $x = 0.05$ and $x = 0.25$; however, the present result does not show such behaviors.

V. DISCUSSION

The present simulation is a very simple one that only takes into account the stabilization of the loop currents. However, it clearly indicates that there two steps for the occurrence of the superconducting phase. First, the phase where the total number of the winding numbers for the loop currents becomes zero appears; next, the phase where the winding number of the loop currents are fixed appears, which we identified as the superconducting phase. The latter phase transition is similar to the one observed in the Berezinskii-Kosterlitz-Thouless transition [17, 18] of the XY model, in which pairs of bound vortices unbind at a critical temperature $T_{\rm BKT}$. In the present case, pairs of bound vortices correspond to pairs of loop currents with winding numbers $+1$ and -1. In the cuprate, the experimental heat capacity is shown to fit very well to the predictions of the three dimensional XY model [19]; thus, the present theory is in accordance with it. Note, however, we only used the optimized χ for Eq. (4) for each combinations of winding numbers $\bar{w}_\ell$ and omit the fluctuations of χ from the optimized value; thus, the calculated heat capacity does not show the behavior of the XY model.

The existence of the two steps for the occurrence of the superconducting phase agreed with the fact that there is a pseudogap phase above the superconducting phase. The present work suggests that in the pseudogap phase, the SVILCs are responsible for the electric current generation, and give rise to the anomalous metallic behavior.

The simulation yields a weak x dependence of T_c with $T_c \approx 0.05t$ for the $U = 8t$ results in Fig. 5**a**; a slightly higher value is obtained for the $U = 6t$ results (Fig. 5**b**). If we substitute $t = 130$ meV, $T_c \approx 0.05t$ yields $T_c \approx 75$ K. This is a reasonable value for the optimal doping.

It is interesting to note that the temperatures scale as $\frac{t^2}{U}$ as is shown in Fig. 5**b**. Since $\frac{4t^2}{U}$ is the exchange parameter for the Heisenberg model derived from the Hubbard model, it is tempting to consider that T_c is related to the spin fluctuation; however, in the present case, it is associated with the fluctuation of the loop currents.

In the cuprates, the superconducting state appear only in the hole doping range, $x_{\rm min} \leq x \leq x_{\rm max}$, where $x_{\rm min} \approx 0.05$ and $x_{\rm max} \approx 0.25$. On the other hand present results show nonzero T_c even at $x = 0.05$ and $x = 0.25$. This disagreement between the present result and experiment will be attributed to the neglect of the temperature and hole concentration dependence of the spin-vortex network formation. Actually, $x_{\rm min}$ is the quan-

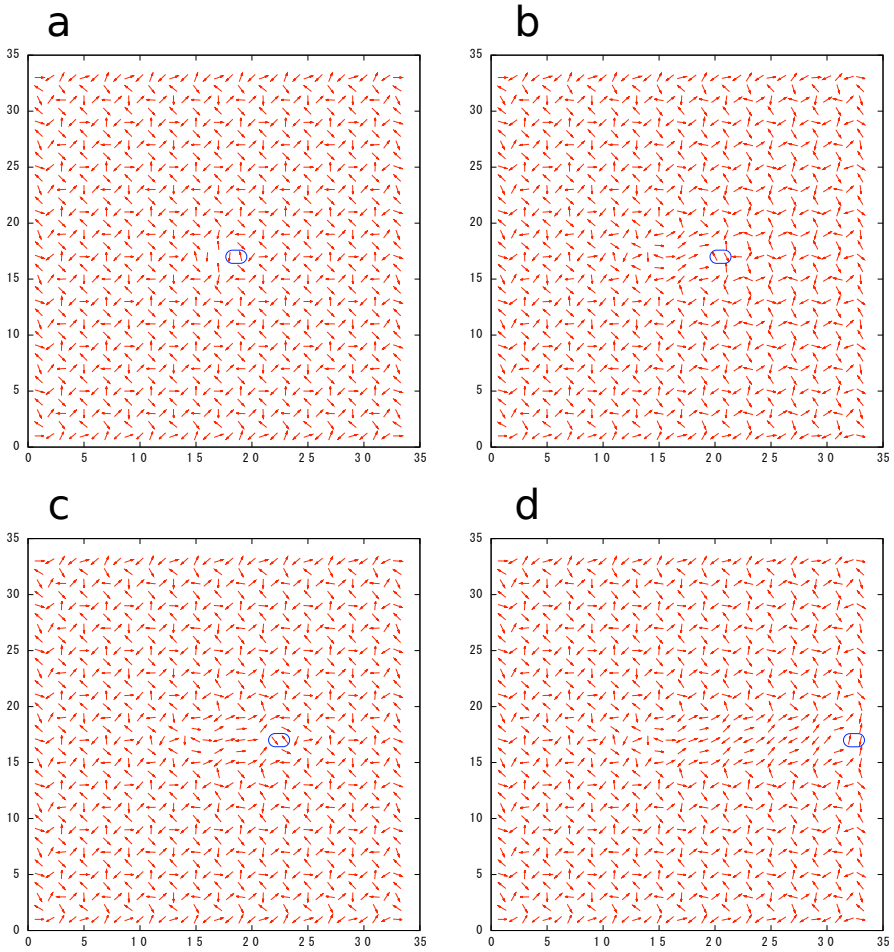

FIG. 6: Destruction of the spin-vortices by adding an extra hole to the state filled with the SVQs. **a**) a hole is added at (17,17) and the spin-vortex around it is destroyed by the energy minimization. **b**) a hole is moved from (17,17) to (19,17), which is accompanied by the destruction of spin-vortices behind; a hole movement is also considered as an electron pair (indicated by the surrounding loop) movement. **c**) a hole is moved to (21,17). **d**) a hole is moved to (31,17).

tum critical point of the insulator-superconductor phase transition, and $x_{\max}$ is that of the superconductor-metal phase transition. Thus, the criticality from these quantum critical points will reduce T_c.

Let us consider the quantum critical point at $x_{\max}$. The resistivity measurement of $La_{1.6-x}Sr_xNd_{0.4}CuO_4$ indicates that $x_{\max}$ is a quantum critical point and the ending point of the pseudogap temperature T^* [20]. In the present theory, the CuO_2 plane is fully covered by SVQs at $x = 0.25$ as seen in Fig. 2**a**. When an extra hole is added to it, the spin-vortices will be destroyed as seen in Fig. 6; if we prohibit the hole arrangement with adjacent hole

pairs due to the Coulomb repulsion between the holes, there is one kind of positions where the extra hole can be added (Fig. 6**a**); when the spin-configuration is optimized after the hole addition, the four spin-vortices around the added hole are destroyed. Now consider the movement of the added hole; the added hole is moved as shown in Fig. 6**b** (to the position where adjacent hole pair does not arise), spin-vortices are further destroyed; when it is moved again (Fig. 6 **c**), it creates behind a ferromagnetic domain (Fig. 6**d**); the electrons in that domain will be a Fermi liquid. By the continuos movement of the adde holes, all the spin-vortices are destroyed.

Although whether the destruction of the spin-vortices are energetically favorable or not cannot be assessed by the present model, the above argument suggests that when holes are added beyond $x = 0.25$, the spin-vortices are destroyed completely at some value of x in the cuprates; if this happens, it becomes the quantum critical point of the spin-vortex formation. We may identify this point to $x_{\rm max} \approx 0.25$ where the superconductor-metal transition also occurs. This superconductor-metal transition is explained as due to the change of the electric current generation mechanism; in $x > x_{\rm max}$ it is the normal one described by the Fermi liquid theory, while in $x < x_{\rm max}$ it is the new one by the spin-vortex-induced loop currents. The current generated by the spin-vortex-induced loop currents explains the anomalous metallic behavior in the pseudogap phase.

Next, let us consider the lowest end point $x = x_{\rm min}$. Many experiments indicate the relation between the percolation of nano-sized superconducting regions is relevant in the cuprate superconductivity [21]. Especially, the STM experiment has observed that the superconducting transition temperature is determined by the percolation of nano-sized superconducting regions [3]. We expect that the SVQ is a stable unit of the spin-vortices, thus, the percolation problem is that of the SVQs. We may estimate this percolation threshold in the following manner: we assume the site percolation of SVQs in the BCC lattice; the threshold value of the site percolation for the bcc lattice is 0.2456; the hole concentration in one SVQ is 0.25; then, the percolation threshold is given by $x = 0.25 \times 0.2456 = 0.0614$, which is a close to the value $x_{\rm min} = 0.05$ observed in the experiment.

Taking into the quantum critical points at $x = x_{\rm min} = 0.05$ and $x = x_{\rm max} = 0.025$, the phase diagram schematically becomes the one in Fig. 7; T_1 in Fig. 5 becomes T_c by including the reduction due to the critical points at $x = x_{\rm min}$ and $x = x_{\rm max}$. On the other hand, $T_{\rm K}$ is obtained from T_2 by taking into account the reduction due to the critical points at $x = x_{\rm max}$

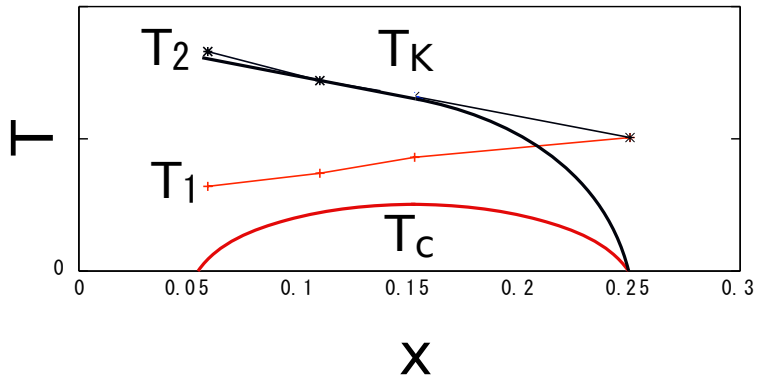

FIG. 7: Schematic picture of the doping dependence of T_c and $T_{\rm K}$. T_1 becomes T_c due to the criticality arising from the quantum critical points at $x = x_{\rm min}$ and $x = x_{\rm max}$. T_2 becomes $T_{\rm K}$ due to the criticality arising from the quantum critical points at $x = x_{\rm max}$.

by assuming that the stability of the spin-vortices are not affected by the formation of the network of themselves.

VI. CONCLUSION

In the present work, we estimate T_c of the hole doped cuprate based on the supercurrent generation mechanism due to the spin-twisting itinerant motion of electrons. The T_c value obtained around the optimum doping agrees reasonably with the experimental value. It scales as t^2/U. The stabilization of the loop currents occurs in two steps when the temperature is decreased; first, the phase where the sum of the winding numbers of the loop currents is zero appears at T_2, second, the phase with the fixed winding numbers for the loop currents appears at T_1. We identify the former to $T_{\rm K}$ and the latter to $T_{\rm c}$. The calculated temperatures disagree with the experimental ones in the underdoped and overdoped regions. These disagreements are due to the neglect of the criticality arising from the quantum critical points at $x_{\rm min}$ and $x_{\rm max}$, where the former is associated with the percolation of the spin-vortices, and the latter with the formation of the spin-vortices.

[1] J. Bardeen, L. N. Cooper, and J. R. Schrieffer, Phys. Rev. **108**, 1175 (1957).

[2] V. J. Emery and S. A. Kivelson, Nature **374**, 434 (1995).

[3] Y. Kohsaka, T. Hanaguri, M. Azuma, M. Takano, J. C. Davis, and H. Takagi, Nature Phys. **8**, 534 (2012).

[4] A. Damascelli, Z. Hussain, and Z.-X. Shen, Rev. Mod. Phys. **75**, 473 (2003).

[5] K. K. Gomes, A. N. Pasupathy, A. Pushp, S. Ono, Y. Ando, and A. Yazdani, Nature **447**, 569 (2007).

[6] J. M. Tranquada, H. Woo, T. G. Perring, H. Goka, G. D. Gu, G. Xu, M. Fujita, and K. Yamada, Nature **429**, 534 (2004).

[7] A. Bianconi, N. L. Saini, A. Lanzara, M. Missori, T. Rossetti, H. Oyanagi, H. Yamaguchi, K. Oka, and T. Ito, Phys. Rev. Lett. **76**, 3412 (1996).

[8] C. J. Zhang and H. Oyanagi, Phys Rev. B **79**, 064521 (2009).

[9] Z. A. Xu, N. P. Ong, Y. Wang, T. Kakeshita, and S. Uchida, Nature **406**, 486 (2000).

[10] J. Xia, E. Schemm, G. Deutscher, S. A. Kivelson, D. A. Bonn, W. H. Hardy, R. Liang, W. Siemons, G. Koster, M. M. Fejer, et al., Phys. Rev. Lett. **100**, 127002 (2008).

[11] H. Koizumi, J. Supercond. Nov. Magn. **24**, 1997 (2011).

[12] R. Hidekata and H. Koizumi, J. Supercond. Nov. Magn. **24**, 2253 (2011).

[13] H. Koizumi, R. Hidekata, A. Okazaki, and M. Tachiki, J Supercond Nov Magn **27**, 121 (2014).

[14] H. Koizumi, A. Okazaki, M. Abou Ghantous, and M. Tachiki, J. Supercond. Nov. Magn. **27**, 2435 (2014).

[15] H. Koizumi and M. Tachiki, J. Supercond. Nov. Magn. **28**, 61 (2015).

[16] H. Koizumi and M. Tachiki, J Supercond Nov Magn 10.1007/s10948-015-3034-5 (2015).

[17] V. L. Berezinskii, Sov. Phys. JETP **34**, 610 (1972).

[18] J. M. Kosterlitz and D. J. Thouless, Journal of Physics C: Solid State Physics **6**, 1181 (1973).

[19] N. Overend, M. A. Howson, and I. D. Lawrie, Phys. Rev. Lett. **72**, 3238 (1994).

[20] O. Cyr-Choinière, R. Daou, J. Chang, F. Laliberté, N. Doiron-Leyraud, D. LeBoeuf, Y. Jo, L. Balicas, J.-Q. Yan, J.-G. Cheng, et al., Physica C **470**, S12 (2010).

[21] N. Poccia, M. Lankhorst, and A. A. Golubov, Physica C **503**, 82 (2014).